

In-situ

3D printing of a carbon fiber reinforced epoxy resin matrix composite using a laser powder bed fusion process



Changchun Chen<sup>a</sup>, Wuxi Xie<sup>b</sup>, Lili Zhang<sup>a\*</sup>, Liang He<sup>c</sup>, Changchun Chen<sup>d</sup>, Lili Zhang<sup>e</sup>, Wuxi Xie<sup>f</sup>, Kang E<sup>g</sup>, Lili Zhang<sup>h</sup>, Xing Gao<sup>i</sup>, Tian Peng<sup>j</sup>

<sup>a</sup> Gemmological Institute, China University of Geosciences, Wuhan 430074, PR China  
<sup>b</sup> Hubei Gem and Jewelry Engineering Technology Research Center, Wuhan 430074, PR China  
<sup>c</sup> School of Materials Science and Engineering, Huazhong University of Science and Technology, Wuhan 430074, PR China  
<sup>d</sup> Mechanical Engineering, University of Birmingham, Birmingham B15 2TT, UK  
<sup>e</sup> School of Electrical and Electronic Engineering, Huazhong University of Science and Technology, Wuhan 430074, PR China  
<sup>f</sup> WMG, Materials Engineering Centre, University of Warwick, CV4 7AL Coventry, UK

ARTICLE INFO

Keywords:

3D printing  
 Carbon fiber  
 SLM  
 CVD  
 EMI

ABSTRACT

Carbon fiber reinforced epoxy resin matrix composite (3DG) was printed using a laser powder bed fusion process. The printed parts were post-processed by chemical vapor deposition (CVD) to improve the mechanical properties. The CVD process was optimized by varying the temperature, time, and atmosphere. The CVD process significantly improved the mechanical properties of the printed parts. The tensile strength of the printed parts increased by 88% and the elongation at break increased by 27% after CVD treatment. The surface energy (SE) of the printed parts increased from 47.8 B to 32.3 B after CVD treatment. The surface energy of the printed parts increased from 2.7 GH to 2–18 GH after CVD treatment. The surface energy of the printed parts increased from 2.7 GH to 2–18 GH after CVD treatment.

1. Introduction

Graphene ( $sp^2$ ) is a two-dimensional carbon-based material with a hexagonal lattice structure. It has a high tensile strength of  $2630 \times 10^9 \text{ N m}^{-2}$  [1], a high thermal conductivity of  $5000 \text{ W m}^{-1} \text{ K}^{-1}$  [2], and a high surface area of  $2630 \text{ m}^2 \text{ g}^{-1}$  [3]. A carbon fiber reinforced epoxy resin matrix composite (3DG) was printed using a laser powder bed fusion process. The printed parts were post-processed by chemical vapor deposition (CVD) to improve the mechanical properties. The CVD process was optimized by varying the temperature, time, and atmosphere. The CVD process significantly improved the mechanical properties of the printed parts. The tensile strength of the printed parts increased by 88% and the elongation at break increased by 27% after CVD treatment. The surface energy (SE) of the printed parts increased from 47.8 B to 32.3 B after CVD treatment. The surface energy of the printed parts increased from 2.7 GH to 2–18 GH after CVD treatment. The surface energy of the printed parts increased from 2.7 GH to 2–18 GH after CVD treatment.

(2DG), 5, 6, 7, 8, 9, 10, 11, 12, 13, 14, 15, 16. B

\*Corresponding author. E-mail address: [zhangll@cug.edu.cn](mailto:zhangll@cug.edu.cn) (L. Zhang).

. T (, fi  
) , fl fi  
(, ) 3DG. B  
3DG w  
(, ). H w  
ffi  
N  
3DG w  
fi 17,18  
H , w  
3DG w  
19  
S (SLM),  
(AM)  
(3D)  
w ffi  
fl *in-situ* T  
SLM T 20  
21 , N 22 . C w  
C w N  
w  
CVD w (< 0.001 %)  
w , w  
23 . W N  
(> 0.1 %) 17 , fi  
24 . H w  
SLM ffi  
w  
fl w w  
(1000–1100 ). F ff  
SLM 25  
T , w fi  
3DG/ (3DG/C )  
SLM w CVD w  
A w  
SLM



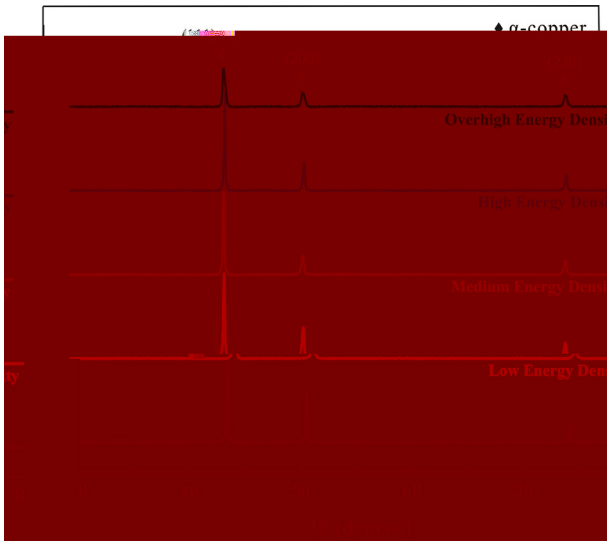


Fig. 3. XRD patterns of  $\alpha$ -copper (Figs. 3 and 4).

3.1.2. Formation of anisotropic microstructure under different volumetric energy density

The XRD patterns of  $\alpha$ -copper (Figs. 3 and 4) show the formation of anisotropic microstructure under different volumetric energy density. The XRD patterns of  $\alpha$ -copper (Figs. 3 and 4) show the formation of anisotropic microstructure under different volumetric energy density. The XRD patterns of  $\alpha$ -copper (Figs. 3 and 4) show the formation of anisotropic microstructure under different volumetric energy density. The XRD patterns of  $\alpha$ -copper (Figs. 3 and 4) show the formation of anisotropic microstructure under different volumetric energy density.

The XRD patterns of  $\alpha$ -copper (Figs. 3 and 4) show the formation of anisotropic microstructure under different volumetric energy density. The XRD patterns of  $\alpha$ -copper (Figs. 3 and 4) show the formation of anisotropic microstructure under different volumetric energy density. The XRD patterns of  $\alpha$ -copper (Figs. 3 and 4) show the formation of anisotropic microstructure under different volumetric energy density. The XRD patterns of  $\alpha$ -copper (Figs. 3 and 4) show the formation of anisotropic microstructure under different volumetric energy density.



Fig. 4. SEM micrographs of SLM-produced copper parts at different energy densities: (a) 3000 J/mm³, (b) 857 J/mm³, (c) 128 J/mm³ (Figs. 3 and 4).

... ..

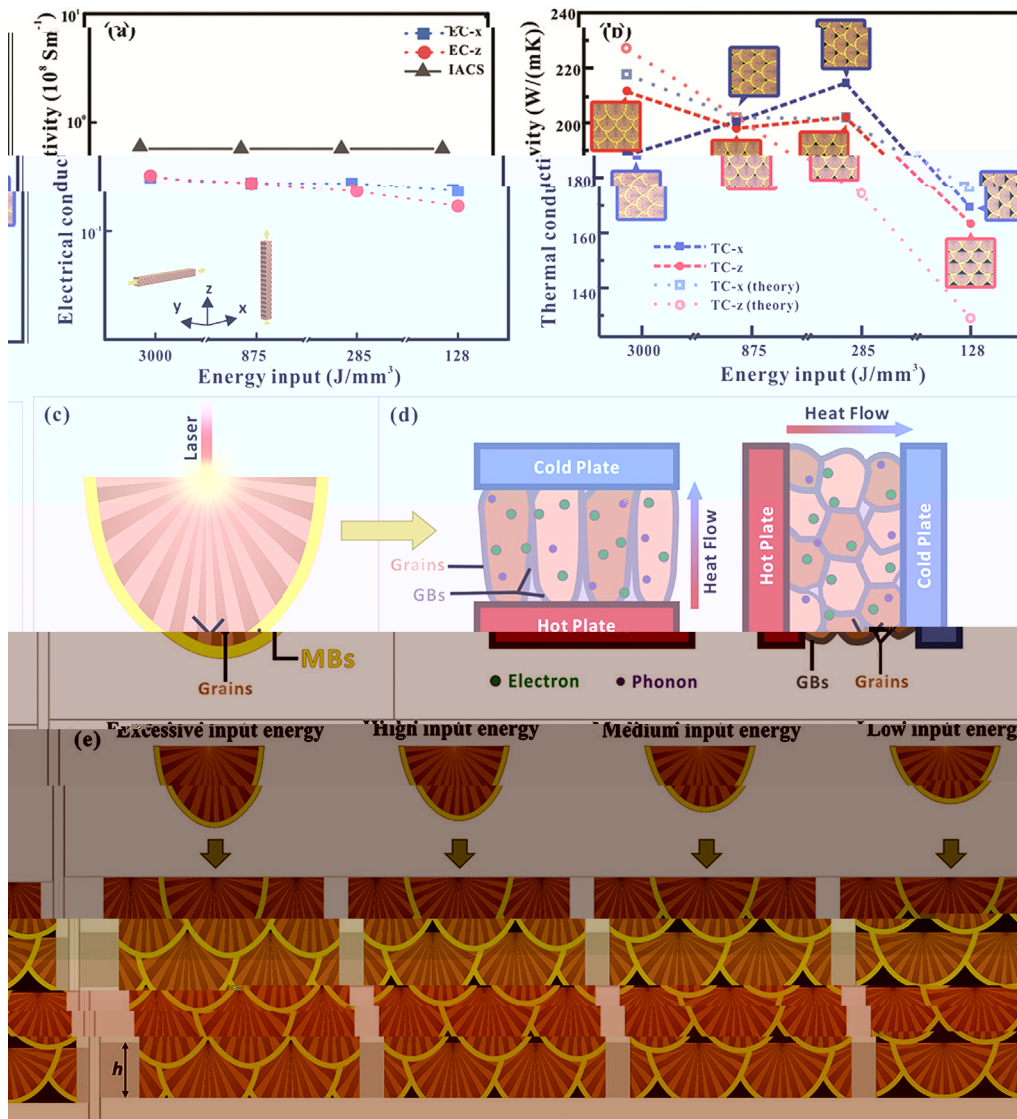


Fig. 7. (a) Electrical conductivity of 3DGC/Cu porous scaffolds with different energy input. (b) Thermal conductivity of 3DGC/Cu porous scaffolds with different energy input. (c) Schematic of laser irradiation on a material. (d) Schematic of heat flow through a material between hot and cold plates, showing electron and phonon transport. (e) Schematic showing the evolution of grain structure from excessive to low input energy.

SEM, with a magnification of 5000 $\times$ . The SEM image shows the porous structure of the 3DGC/Cu porous scaffold, with a pore size of approximately 450  $\mu\text{m}$  (Fig. 8a). The porous structure is composed of interconnected fibers, and the pore size is uniform. The SEM image also shows the surface morphology of the porous scaffold, which is highly porous and interconnected.

### 3.3. Morphology and structure of CVD 3DG/Cu porous scaffolds

The morphology and structure of the CVD 3DG/Cu porous scaffolds were investigated using SEM and EDS. The SEM images show the porous structure of the scaffolds, with a pore size of approximately 450  $\mu\text{m}$  (Fig. 8a). The porous structure is composed of interconnected fibers, and the pore size is uniform. The SEM image also shows the surface morphology of the porous scaffold, which is highly porous and interconnected. The EDS analysis shows the presence of carbon and copper in the scaffolds, indicating the successful synthesis of the CVD 3DG/Cu porous scaffolds. The porous structure of the scaffolds is highly porous and interconnected, which is beneficial for the application of the scaffolds in various fields.

The porous structure of the scaffolds is highly porous and interconnected, which is beneficial for the application of the scaffolds in various fields. The SEM images show the porous structure of the scaffolds, with a pore size of approximately 450  $\mu\text{m}$  (Fig. 8a). The porous structure is composed of interconnected fibers, and the pore size is uniform. The SEM image also shows the surface morphology of the porous scaffold, which is highly porous and interconnected. The EDS analysis shows the presence of carbon and copper in the scaffolds, indicating the successful synthesis of the CVD 3DG/Cu porous scaffolds. The porous structure of the scaffolds is highly porous and interconnected, which is beneficial for the application of the scaffolds in various fields.





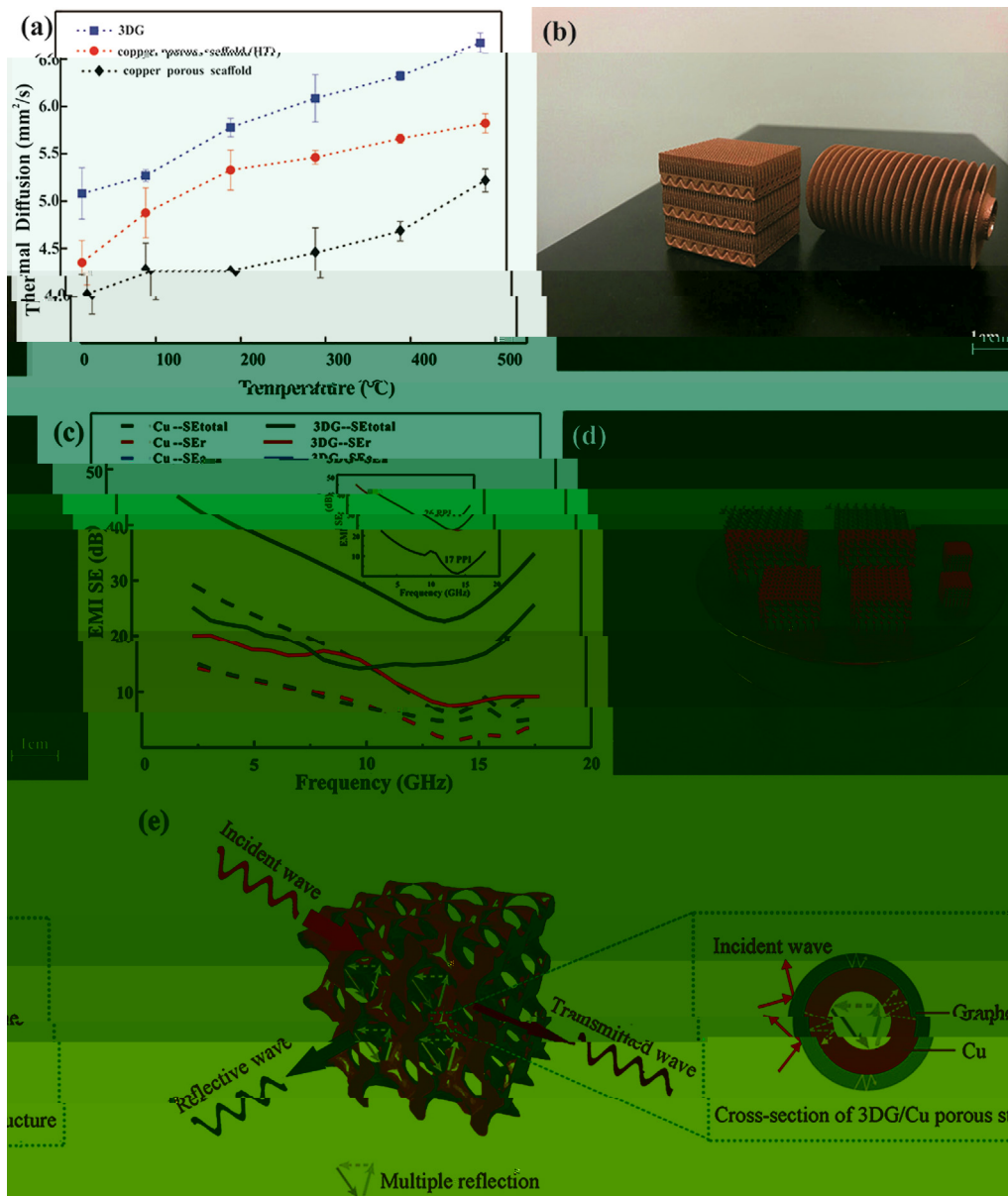


Fig. 9. (a) Thermal Diffusion of 3DG/Cu porous scaffold (□) and copper porous scaffold (○) SLM fabricated porous scaffold (HT) (●) and copper porous scaffold (●). (b) 3D models of 3DG and copper porous scaffold. (c) EMI SE of 3DG/Cu porous scaffold (□) and copper porous scaffold (○) SLM fabricated porous scaffold (HT) (●) and copper porous scaffold (●). (d) 3D model of the porous structure. (e) Schematic of wave interaction with the porous structure showing incident, reflective, and transmitted waves, and a cross-section of the 3DG/Cu porous structure.

Table 1

Comparison of EMI SE and improvement of thermal property for various porous structures.

Coating materials	Substrate	Method	Maximum shielding efficiency (dB)	Improvement of thermal property (%)	Ref
G	G	I	37	-	50
G	PS	H	29.3	-	56
G	PMMA	S	19	-	57
C /G	A	S	-	8.5	58
G	N	F	-	554	59
G	C-N	E	20	-	60
G	C	P	-	2.4	61
G	C	F	47	6.3	62
G	C	CVD + SLM	47.8	27	T

Note: (□) -PPMA, (○) -PS.



HT  
*in-situ* w (F. 9a). S  
 3DG/C ff  
 HT  
 1-2  
 SLM  
 fl w (w fl SLM  
 500 μm)  
 (F. 9b),  
 G  
 (T. 1). I  
 O  
 T  
 EMI, EMI SE, w 3DG/C ff  
 (EM) w  
 2-18 GHz (F. 9c),  
 W *in-situ* w  
 ff SE 15.9 32.3 B, w  
 47.8 B (88.2% ),  
 20 B. T  
 3DG/C fi w  
 J K 44 EMI  
 w T EMI SE  
 133% ) 20 110 PPI ( ).  
 R K 45 EMI  
 W  
 17 26 PPI (F. 9c insert) 105%  
 EMI SE. I w EMI  
 ff w SLM. T  
 3DG/C 26 PPI EMI SE  
 32.3 B, 99.9% EMI w T  
 60  
 (30 ff ) 46 T EMI  
 3DG/C w  
 T 1. I EMI SE  
 3DG/C w  
 3D  
 T EMI fl (SE<sub>r</sub>),  
 (SE<sub>a</sub>) fl (EM) w 47,  
 w  
 48 R 49 w  
 w, w  
 T w EM w  
 fi  
 50 R EMI  
 T  
 w w w  
 w fi C 51 F  
 w  
 52 S O<sub>2</sub> 53 W  
 3DG/C ff w

SE<sub>r</sub>, SE<sub>a</sub>, w F. 9e. W w  
 w 3DG/C ff  
 w w fl w  
 w w ff S  
 3DG/C  
 fl  
 w w T  
 EM w fi w  
 w EM w  
 SE<sub>r</sub>, O  
 w ff, w w fi EM  
 w ff EM  
 T  
 ff w  
 w J 54 I w  
 fi w  
 fl ff M  
 w  
 w fl  
 EM w  
 EM w T w  
 w 44 T  
 w 3D EM w w  
 I CVD  
 R S 3.3  
 EM w w  
 55 I  
 O w  
 3DG/C  
 fi w fi  
 T  
 w ff

4. Conclusions

A 3DG/C ff w w  
*in-situ* CVD  
 T ff W  
 3DG/C EMI SE  
 15.9 ( ) 32.3 B,  
 47.8 B (88.2% ), w 26.8%  
 ff T 3DG/C  
 ff fl fi  
 T EMI  
 3DG/C ff  
 EMI

Credit authorship contribution statement

Kaka Cheng: C, M, F  
 Wei Xiong: V, I, W  
 Yan Li: W &, F  
 Liang Hao: F  
 Chunze Yan: R, F  
 Zhaoqing Li: V  
 Zhufeng Liu: F  
 Yushen Wang: I, S  
 Khamis Essa: W &  
 Li Lee: D  
 Xin Gong: S  
 Ton Peijs: W &, S

Declaration of Competing Interest

T... fl...

Acknowledgement

T... w... fi... N... N... S... F... C... (N... 51671091, N... 51902295, N... 51675496). T... F... R... F... C... U... C... U... G... (W... ) (N... CUG170677), H... P... N... S... F... (N... 2019 CFB264).

Appendix A. Supplementary data

S... // /10.1016/... .2020.105904.

References

- B... N... N... M... K... M... S... G... ACS N... 2018;91:24-69.
- B... AA, G... S, B... W, C... L, T... W... D, M... F... S... ACS N... 2008;8(3):902-7.
- L... H, C... M, P... w... H, P... O, S... G... ACS A... M... 2016;8(36):24112-22.
- K... M, K... J, J... B, C... K... JH, A... JH, G... ACS N... 2017;11(8):7950-7.
- P... C... M, H... M, T... M... L... D... P... ACS N... 2020;262:118266-76.
- L... XJ, W... C... LL, J... SH, W... G... L... F... C-G... ACS N... 2017;101:50-8.
- HQ, L... SW, C... LH, J... SH, H... HQ, S... ACS N... 2018;6(42):21216-24.
- D... TM, S... P, D... P, K... J, Kw... M, A... T... ACS N... 2017;1(4):467-70.
- Q... L, L... L... T... ACS A... 2014;4(72):38273-80.
- D... X, H... L... SP, N... W... JG, 3D... ACS N... 2016;90:424-32.
- L... XL, XW, S... CO, H... MK, X... HL, D... W... ACS N... 2018;10(1002):201803938.
- L... J, P... X... C, R... G... N... D... G... ACS N... 2013;7(7):6001-6.
- J... SH, A... w... S, G... A... L... w... ACS N... 2017;56:15520-38.
- I... T... S... w... K, K... M, T... T... T... K... ACS N... 2018;20(9):6024-33.
- S... K, D... N... M... C... V... N... E... J... T... ACS N... 2002;149(8):370-7.
- C... XH, S... M, S... WH, L... G, H... X... Q... ACS N... 2011;7(22):3163-8.
- K... H, G... M, J... I, H... J, W... C... C... M... U... ACS N... 2019;1(4):1077-87.
- S... Q... F... X, L... W, L... H... L... ACS N... 2017;29(31):1701583-90.
- X... X, G... C, X... L... T... H... D... W... ACS N... 2019;10(1021):1908191.
- C... C, H... B... X, N... J, C... S, L... F... ACS N... 2019;175:107824-33.
- S... ěĀ, B... ěĀ, D... T... ff... ACS N... 2016;307:407-17.

- R... DC, HB, L... J, L... SJ, J... W... ACS N... 2020;771:138586-95.
- L... X, C... W, A... J, K... S, N... J... ACS N... 2009;324(5932):1312-4.
- C... P, R... WC, G... LB, L... BL, P... SE, C... HM, T... ACS N... 2011;10:424-8.
- J... SD, D... S, G... L, K... JP, H... JV, V... ACS N... 2019;270:47-58.
- X... W, H... L, L... T... D, C... Q, F... ACS N... 2019;170:107697-708.
- G... DD, M... W, W... K, P... ACS N... 2013;57(3):133-64.
- L... E, T... S, C... L, F... ACS N... 2017;249:255-63.
- X... S, W... L, J, W... P, C... ACS N... 2018;124:685-98.
- L... M... S, D... W, S... C... ACS N... 2015;87:797-806.
- L... CLA, M... S, T... w... M, A... w... RC, W... PJ, L... PD, T... ACS N... 2019;166:294-305.
- T... X, K... T... WQ, T... J, D... M, M... D... ACS N... 2016;6:26039-48.
- K... H, T... XP, L... NH, T... SB, C... CK, G... ACS N... 2016;11(3):183-91.
- R... fi HK, K... NV, G... H, S... TL, S... ACS N... 2013;22(12):3872-83.
- T... X, K... T... J, V... G, P... QX, G... ACS N... 2015;646:303-9.
- R... DA, M... LE, M... H... ACS N... 2011;59(10):4088-99.
- X... W... H... ACS N... 2018;743:258-61.
- K... S... W... ACS N... 2003;23:309-48.
- L... G... G... J... ff... R... G... N... ACS N... 2010;10(9):3512-6.
- L... XS, C... WW, C... L... R... ff... R... S... E... ACS N... 2009;9(12):4268-72.
- X... W, X... C... X... W... H... SQ... ACS N... 2020;161:479-85.
- F... AC, M... JC, S... V... C... C... L... M... M... F... ACS N... 2006;97(18):187401-4.
- S... G... J... SH, F... PC, H... HQ, F... ACS N... 2017;200:97-100.
- J... K... H... J... C... J... D... F... ACS N... 2014;311:351-6.
- R... K... M... DP, A... C... M... S... S... K... E... ACS N... 2018;12:475-84.
- S... B... L... W... W... C... ACS N... 2016;8(12):8050-7.
- L... N... H... D... F... H... X... L... X... G... S... H... E... H... H... ACS N... 2016;307:407-17.

M 2019;34(5):489–98.

53 W B, C M, L M. R. *Composites Part A* 2014;26:3484–9.

54 C H, W S, J J, X C, J S. *Composites Part A* 2019;121:139–48.

55 W L, J Q, T ff MWCNT. *Composites Part A* 2015;26(3):1895–9.

56 D X, P GR, H P, Q F, M B. *Composites Part A* 2012;22:1877–4.

57 HB, Q, WG, H X, T. *Composites Part A* 2011;3:918–24.

58 S A, U N, T V. T. *Composites Part A* 2016. [:// doi.org/10.1051/compta/2016021](https://doi.org/10.1051/compta/2016021).

59 P MT, J H, R ff RS, S L. T. *Composites Part A* 2012;12:2959–64.

60 J K, H, H, D P. *Composites Part A* 2017;122:244–7.

61 R H, L S, B S, K TW, L DS, L HJ, T. *Composites Part A* 2015. [:// doi.org/10.1038/ncomms12710](https://doi.org/10.1038/ncomms12710).

62 XT, F SG, L G, Q, L G, R KP, S. *Composites Part A* 2020. [:// doi.org/10.1016/j.compta.2019.105670](https://doi.org/10.1016/j.compta.2019.105670).

63 R DA, M LE, M E, H DH, M JL, M BI, N. *Composites Part A* 2011;59(10):4088–99.

64 E SF, L KG, S VK, M IC. T. *Composites Part A* 1973;1(1):10–38.